Inorganic Chemistry

Article

pubs.acs.org/IC

Biphasic MO_{2+x}–M_3O_{8-z} Domain of the U–Pu–O Phase Diagram

Michal Strach,*[,†,‡] Renaud C. Belin,*[,†] Jean-Christophe Richaud,[†] and Jacques Rogez[‡]

[†]CEA, DEN, DTEC, SECA, LCC, Cadarache F-13108 Saint-Paul-Lez-Durance, France

[‡]IM2NP, UMR 6122, CNRS, Aix Marseille University, Case 251, Avenue Escadrille Normandie Niemen, 13397 Marseille Cedex 20, France

ABSTRACT: The reduction of six mixed-oxide samples containing 14, 24, 35, 46, 54, and 62 mol % Pu was studied in situ by X-ray diffraction. The samples were first oxidized in air and subsequently reduced in a controlled atmosphere corresponding to a stoichiometric composition with an O/M = 2.00. After oxidation, we observed two structures, one cubic and one orthorhombic, MO_{2+x} and M_3O_{8-z}. The two phases were subsequently reduced back to their stoichiometric O/M = 2.00 in a controlled atmosphere. The plutonium contents of the two resulting cubic structures differed from the initial one. We conclude that strong cation transport took place during oxidation, according to the shape of the tie lines in the biphasic MO_{2+x}/M_4O_9–M_3O_{8-z} domain. The resulting overall O/M after oxidation was estimated. We propose the shape of the tie lines in the aforementioned biphasic domain and suggest a maximal plutonium solubility in the M_3O_8 structure at 8 ± 2 mol % (Pu/U + Pu) at 1573 K.

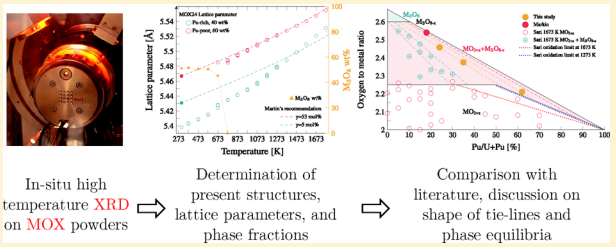

INTRODUCTION

Uranium oxides bearing certain amounts of plutonium (Pu) are considered for use in both conventional reactors and fast breeders, depending on the composition.[1] Although the understanding of the U–Pu–O system is advanced at this point, there still exist certain regions on the phase diagram, where uncertainties prevail. This is the case for the hyper-stoichiometric UO_2–PuO_2–U_3O_8 region of the diagram, especially for high Pu contents and elevated temperatures. The complex appearance of this region proposed in previous studies, caused by the existence of various oxygen (O)-rich phases such as M_3O_7, M_4O_9, or M_3O_8, makes it particularly hard to study. It has been found that the physical and chemical properties of the compound in question change with the oxygen-to-metal ratio (O/M), and thus it is of importance to precisely determine the thermodynamic properties of MOX materials at O/M > 2.00.

In a previous study,[2] we explored the possibility of in situ X-ray diffraction studies on the oxidation products and kinetics of the UO_2–PuO_2–U_3O_8 domain. There are certain advantages of in situ studies over ex situ examinations, which motivate development in this field. In the case of the studied oxides, it has been shown that, even at low temperatures, we can anticipate reactions with the surrounding atmosphere,[3] which might introduce error into the postexamination after quenching. Also, the complex behavior of MOX during reduction and oxidation involves subtle changes in the properties, which might be hard to spot ex situ. It is also evident that in the case of active materials the sample preparation procedures are cumbersome and require dedicated handling equipment. The preparation of numerous samples to study phase diagram domains can be omitted by modifying the composition of one sample in situ by controlling the oxygen potential of the gas used. Taking the success of the previous study in helping to determine the oxidation behavior of MOX samples with various Pu contents, we continue to develop this approach with another campaign. Here we hope to address the issues that became apparent after the first series of experiments, namely, the swelling of samples and lack of data on the composition of the constituting structures.

We focus on the biphasic MO_{2+x}/M_4O_9 + M_3O_{8-z} domain at elevated temperatures, which was previously reported in various studies.[4−6] The boundaries of this domain were described to lie between O/M = 2.28 and 2.61 and up to $y = 0.5$ ($y = x_{Pu}/x_U + x_{Pu}$). Benedict and Sari[7] concluded that the orthorhombic phase remains poor in Pu and the actinide is mostly present in the face-centered-cubic (fcc) phase. Meanwhile, Markin and Street[4] postulated that the Pu/U ratio in this biphasic region remains constant for compositions with $y \leq 0.3$. In the phase diagram published by Sari et al.,[5] a M_3O_8 + MO_{2+x} region was defined between $(U_{0.95}Pu_{0.05})_3O_8$, $(U_{0.4}Pu_{0.6})O_{2.24}$, and $(U_{0.65}Pu_{0.35})$-$O_{2.25}$. Markin and Street[4] also proposed such a domain, postulating a certain cation disproportionation. For example, for the overall $y = 0.18$, the M_3O_8 phase was assumed to contain 9% Pu, while the MO_{2+x} contained 84–88%. As for the O-rich single-phase regions, a M_3O_8 phase domain at O/M > 2.61 was observed. The plutonium solubility in this phase was reported to be limited to 6% and its O content constant with increasing Pu doping.[7] Markin and Street did not exactly determine the maximum Pu content for this phase but placed it at around Pu/(Pu + U) = 0.35 and observed that the O content decreases with increased Pu doping. With further Pu addition ($y > 0.5$), Dean[8] and Brett and Fox[6] found a single fluorite

Received: July 10, 2015
Published: September 11, 2015

DOI: 10.1021/acs.inorgchem.5b01544
Inorg. Chem. 2015, 54, 9105–9114

phase below the line joining the $UO_{2.5}$ and PuO_2 compositions. This line is considered to be the limit of oxidation of the considered mixed oxide in air.

In this study, the products of oxidation and the process of reduction were studied for six samples with different Pu contents. The obtained patterns were used to determine the lattice parameter evolution of the cubic phases and phase fractions if more than one structure was observed. From this analysis, we draw conclusions on the phase boundaries in the UO_2−PuO_2−U_3O_8 region and some thermodynamic properties of the products of oxidation. We also discuss the kinetics of the changes in O/M and compare our results with the ones found in the literature.

MATERIALS AND METHODS

We studied six MOX samples with different Pu compositions, namely, 14, 24, 35, 46, 54, and 62 mol % Pu. The pellets were fabricated from coground UO_2 and PuO_2 powders and sintered in an atmosphere corresponding to a stoichiometric composition. The fabrication process was described in detail by Truphémus et al.[9]

Data acquisition was carried out using a Bruker D8 Advanced X-ray diffractometer with copper radiation form a conventional tube source in a Bragg−Brentano θ−θ configuration. The powdered samples were inserted on a platinum heating strip in a MTC-HIGHTEMP+ chamber and stage. A temperature calibration was carried out for the two gases used, air and purified helium. We consider that the slight changes in the composition of the gas during heat treatments (oxygen partial pressure decreasing from 10^{-24} to 10^{-27} measured at 923 K) did not affect the temperature measurement. We estimate the error on the temperature values at ±15 K.

The experimental work consisted of two parts. First, all of the samples were oxidized in air at 1573 K for 5 h except for the least Pu-doped sample, which was treated at 1373 K for 3 h. The temperatures and durations were chosen based on previous results recorded during the gradual oxidation of the same MOX compounds as those used here.[2] The highest observed quantities of M_3O_8, and what follows, the highest O/M between room temperature and 1773 K, were observed between 1300 and 1400 K. We chose a slightly lower temperature in the case of MOX14 because the oxidation of this compound results in high amounts of M_3O_8, thus making the sample susceptible to premelting processes. The treatment used was comprised of fast heating at 5 deg/s to the intended temperature, isothermal plateau, and subsequent fast cooling at the same rate. Afterward, the treated powder was removed from the heating strip, milled in an agate mortar, and stored for 1−5 days, before the reducing treatment. Grinding, redeposition of the oxidized powder, and carrying out a new calibration made it possible to observe the present structures without the errors stemming from swelling. This was discussed in detail in the previous study and has a strong effect, especially for uranium (U)-rich samples. The thermal profile used in this case is shown in Figure 1 and was the same for all samples, except MOX14, in which case the sample was heated and cooled with four scans every 100 deg (2 h per isothermal plateau for each 100 deg) up to 1573 K. During reduction, we used a conventional He bottle containing small amounts of impurities H_2O < 0.5 ppm, O_2 < 0.1 ppm, CO < 0.1 ppm, and H_2 < 0.1 ppm. Untreated, the oxygen partial pressure in this mixture is 10^{-4} atm. Using a commercially available Setnag Gen'Air oxygen pump, we decreased the amount of O to a level where it began to be governed by the $H_2 + O_2 \leftrightarrow H_2O$ reaction and achieved a partial pressure of 10^{-27} atm, measured by an oxygen probe at 923 K.

Patterns were acquired in the 25° < 2θ < 140° angular range at 0.02°/0.3 s. Thus, a full scan was achieved in about 25 min. To treat the data, *TOPAS 4.0*[10] software was used. Signal contributions coming from the geometry, tube type, and slits were included in the fitting according to the fundamental parameter approach. All patterns were fitted using the Rietveld approach,[12] with the background to noise approximated by a Chebyshev function with three terms. Contributions from the microstructure were simulated by a physical broadening function. We estimated the error on the lattice parameter determination at 10^{-3} Å and the weight percent at ±3 wt %. Although it has been reported that the product of oxidation in MOX might be M_4O_9 with a distinct structure, it surely is similar to the basic fluorite one for stoichiometric materials, and thus we chose to fit the pattern using the $Fm\bar{3}m$ structure. A more detailed reasoning for choosing this structure instead of the other one can be found in our previous work.[2] As for the M_3O_8 structure, we use either the hexagonal $P\bar{6}2m$ or the orthorhombic $C2mm$, depending on the temperature.

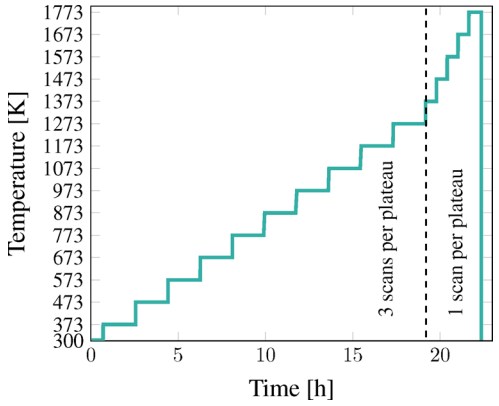

Figure 1. Temperature profile used for MOX24−MOX62 reducing treatments.

RESULTS

Here we give a detailed description of evolution of the cubic lattice parameters from this and, in some cases, the previous study,[2] weight percent of the hexagonal phase, and Martin's recommendation[11] for stoichiometric compounds. The equation taken from ref 11 is as follows:

at 273 < T < 923 K

$$a = a_{273}(9.973 \times 10^{-1} + 9.802 \times 10^{-6}T - 2.705 \times 10^{-10}T^2 + 4.931 \times 10^{-13}T^3)\ [\text{Å}] \quad (1)$$

at 923 < T < 3120 K

$$a = a_{273}(9.9672 \times 10^{-1} + 1.179 \times 10^{-5}T - 2.429 \times 10^{-9}T^2 + 1.219 \times 10^{-12}T^3)\ [\text{Å}] \quad (2)$$

where a is the lattice parameter at T and a_{273} is the lattice parameter at 273 K. The lattice parameters in most cases seem to follow Martin's recommendation for thermal expansion of a stoichiometric MOX. On the basis of several studies, Martin concluded that UO_2 and PuO_2 expand almost identically in temperature as long as they are stoichiometric. Thus, there exists just one expression for the coefficient of thermal expansion independent of the U/Pu ratio in $(U,Pu)O_2$. It makes it reasonable to consider that if a given MOX cubic structure follows Martin's recommendation, it is stoichiometric because oxygen defects accompanying departure from stoichiometry were shown to induce a strong change in the expansion of MOX.[2]

We assume that, after the reducing treatment, the two structures, which were a product of oxidation, came back or close to stoichiometry: $M'O_{2+x} \rightarrow M'O_2$ and $M_3''O_8 \rightarrow M''O_2$, with $y_{M'} > y_{M''}$ (where $y_{M'/M''}$ is the $x_{Pu}/x_U + x_{Pu}$ ratio in each structure). We estimate the Pu content of the stoichiometric structures after reduction by comparing their lattice parameters to Vegard's law.

DOI: 10.1021/acs.inorgchem.5b01544
Inorg. Chem. 2015, 54, 9105−9114

In Figures 2 and 3, we show stack plots of diffraction patterns taken respectively before and after the reducing heat treatment for all of the studied samples.

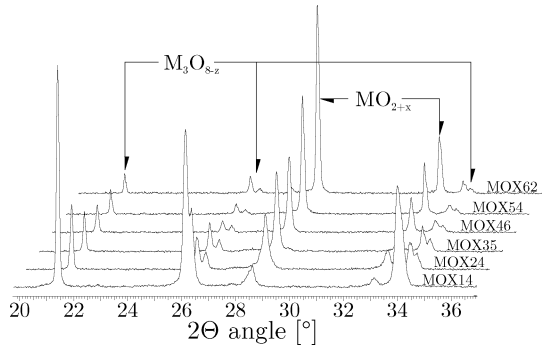

Figure 2. Diffraction patterns taken before the reducing heat treatment.

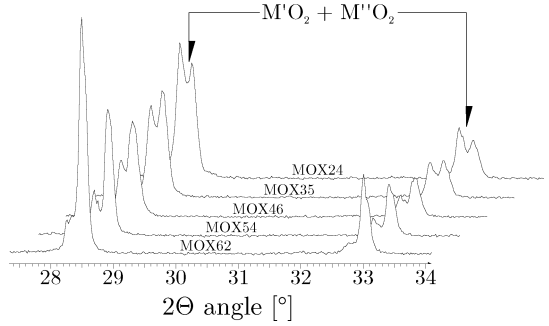

Figure 3. Diffraction patterns taken after the reducing heat treatment.

Lattice parameter evolution of the cubic structure and the M_3O_8 weight percent were plotted as a function of the temperature for all of the studied samples in Figures 5−9. We list the lattice parameters of $M'O_{2+x}$ after oxidation and $M''O_2$ and $M'O_2$ after reduction in Table 1. The weight fractions and Pu contents are given in Table 2.

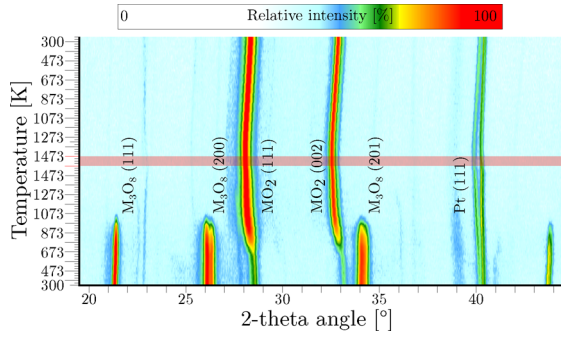

Figure 4. Isointensity map for MOX14. Each horizontal slice corresponds to a pattern recorded at a given temperature during the reducing heat treatment. The horizontal colored zone corresponds to the 1573 K plateau.

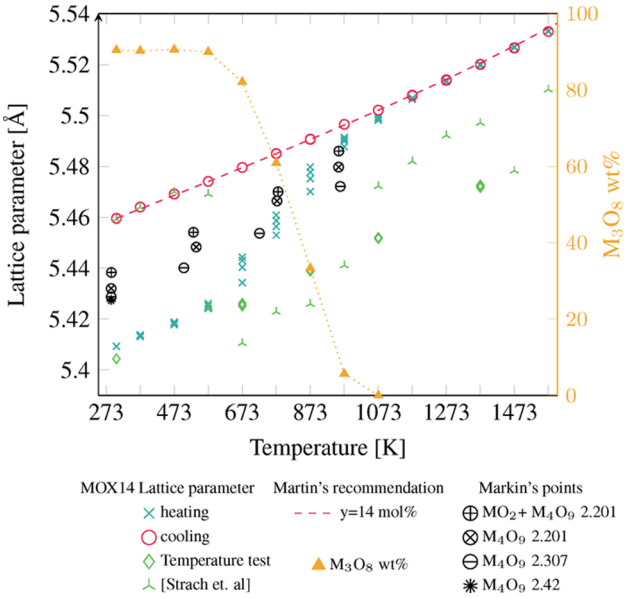

Figure 5. Lattice parameter evolution and M_3O_8 weight percent during the reducing heat treatment for MOX14. The M_3O_8 weight percent corresponds only to heating. The dashed line is Martin's[11] recommendation for thermal expansion for stoichiometric MOX with 15 mol % Pu (Pu/U + Pu). Four series of points were taken from ref 4 for biphasic samples with y = 0.15 and overall O/M noted in the figure together with the structures. Data from ref 2 recorded during heating under air was added. Lattice parameters observed for the same oxidized MOX14 powder used later in the reduction experiment, which was ground, positioned on the heating strip, heated once again to 1373 K, and then cooled to 1073, 873, 673 K with 4 h at each temperature, constitute the temperature test series.

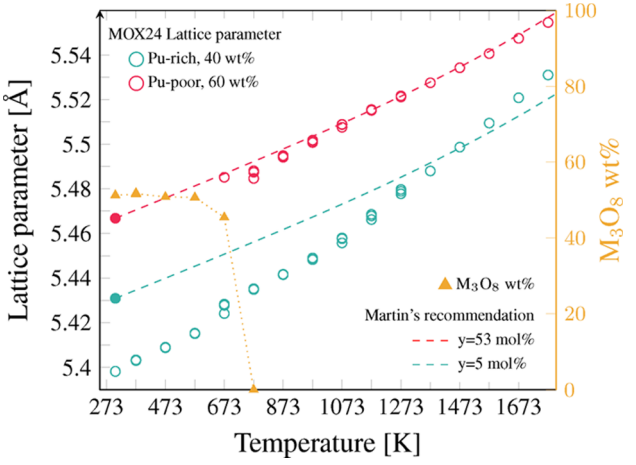

Figure 6. Lattice parameter evolution and M_3O_8 weight percent plotted in temperature during the reducing heat treatment [$T = f(t)$ in Figure 1] for sample MOX24. The two dashed lines correspond to Martin's[11] recommendations for thermal expansion of stoichiometric MOX compounds with Pu contents estimated by comparing the final lattice parameters measured after reduction (colored points) with Vegard's law.

MOX14. What can be concluded from the evolution of the diffraction patterns is that the oxidation of MOX with 14 mol % Pu in air at 1373 K resulted in the formation of two structures, which upon reduction form once again one structure. This becomes clear when we look at the isointensity map for this thermal cycle in Figure 4. It is further discussed in the Reduction section.

The lattice parameter of the cubic structure after reduction was observed to be 5.409 Å. It is much lower than 5.428 Å observed by Markin and Street, supposedly for a MOX sample

DOI: 10.1021/acs.inorgchem.5b01544
Inorg. Chem. 2015, 54, 9105−9114

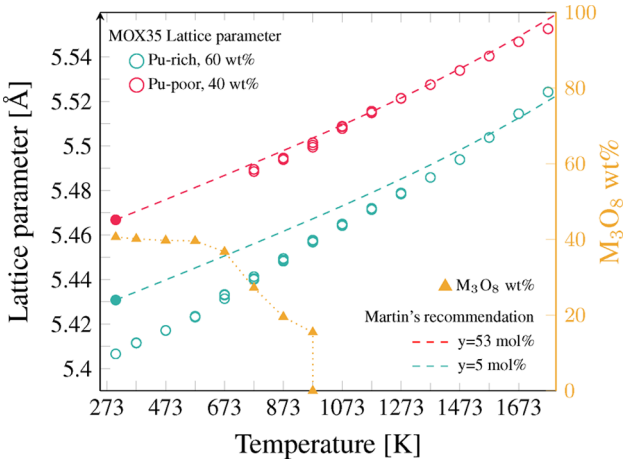

Figure 7. Lattice parameter evolution and M_3O_8 weight percent plotted in temperature for MOX35. See the caption of Figure 6.

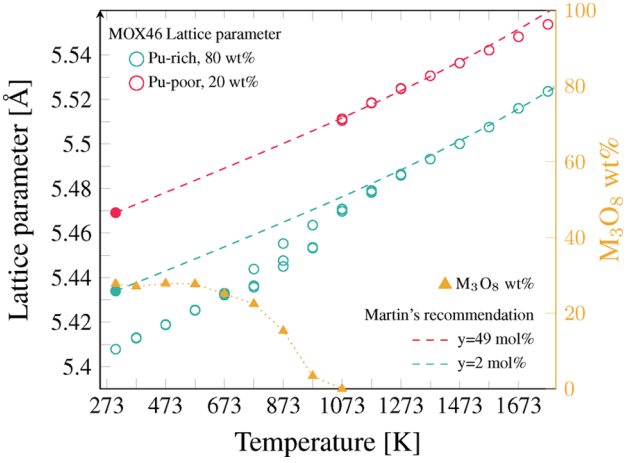

Figure 8. Lattice parameter evolution and M_3O_8 weight percent plotted in temperature for MOX46. See the caption of Figure 6.

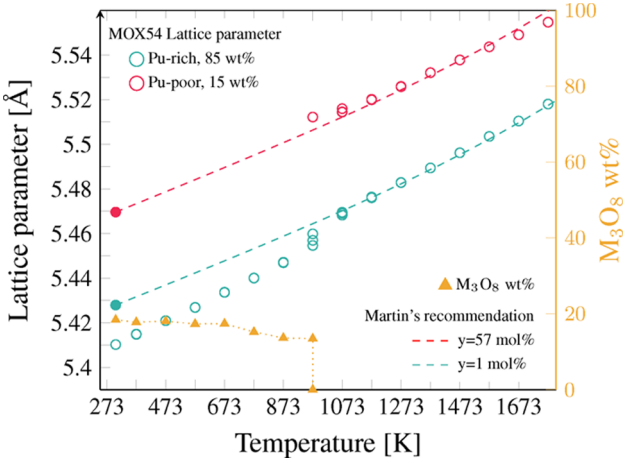

Figure 9. Lattice parameter evolution and M_3O_8 weight percent plotted in temperature for MOX54. See the caption of Figure 6.

containing also 15 mol % Pu and oxidized to an overall O/M = 2.42.

The sample started to lose O between 573 and 673 K, which affected both the lattice parameter and the weight percent. The dashed line in Figure 5 corresponds to a recommendation made by Martin[11] for thermal expansion of the stoichiometric MOX compounds, in this case MOX with 15 mol % Pu (Pu/U + Pu).

Table 1. Lattice Parameters of Cubic Structures before and after the Reducing Heat Treatment

sample	$M'O_{2+x}$	$M'O_2$	$M''O_2$
MOX14	5.408	5.459	
MOX24	5.396	5.467	5.429
MOX35	5.406	5.43	5.467
MOX46	5.407	5.434	5.469
MOX54	5.41	5.428	5.469
MOX62	5.404	5.42	5.465

During heating, the lattice parameters start to follow this line from 1173 K. Also, afterward, during the remaining heating and during the whole cooling period, we observe a similar correspondence. The sample became stoichiometric at 1173 K, and afterward, O/M did not vary during the remaining time of the experiment. Most likely, the full reduction would have taken place at a lower temperature, judging from the evolution of the lattice parameters at each isothermal plateau. Between 573 and 1173 K, the plateaus might have been too short for the sample to equilibrate with the gas. For comparison, we have also added the lattice parameters recorded during an experimental campaign described in detail in ref 2. The values are much lower, which was most likely caused by the swelling of powder due to oxidation (the hexagonal structure has a much higher cell volume than the cubic one). This effect changes the physical properties of the studied material, yielding the initial configuration (Z adjustment and rocking curve) invalid. From this comparison, the advantage of the described approach becomes clear. We do not observe swelling of the sample during the reduction, and thus the patterns remain unaffected, which was not the case in the previous experimental campaign.

We also add results from an experiment carried out in air, where the oxidized MOX14 sample (1373 K for 2.5 h in air) was heated once again to 1373 K and then cooled to 1073, 873, and 673 K with 4 h at each temperature (temperature test data series). Throughout this treatment, the ratio between the cubic and M_3O_8 weight percent remained constant and evolution of the cubic lattice parameter was slightly steeper than that in Martin's recommendation for a stoichiometric MOX. Thus, we can conclude that no O/M changes occurred during this treatment, which confirms our correct choice of temperature and duration for the oxidizing treatment.

MOX24. Reduction began at 673 K, with the M_3O_8 reflections disappearing at 773 K. In this case, the Pu-rich cubic phase was apparently reduced to an O/M below the stoichiometric composition and/or the Pu content was reduced slightly, with the lattice parameter going above that of Martin's recommendation at 1473 K. The latter is rather unlikely because evolution of the lattice parameter of the other observed structure did not vary at all from that of Martin's recommendation. There is also a possibility that sintering might have started and premelting processes induced a change in the physical properties of the sample, causing a shift of the lattice parameter, but once again the second phase seemed unaffected. We conclude that the Pu-poor cubic phase, which formed after the reduction of M_3O_8, had a lattice parameter corresponding to that of a stoichiometric MOX with 4.5 mol % Pu throughout the heat treatment, based on the fact that it followed Martin's recommendation. At the end of the reducing heat treatment, the fraction of the Pu-poor to -rich structure

DOI: 10.1021/acs.inorgchem.5b01544
Inorg. Chem. 2015, 54, 9105−9114

Table 2. y_{init} Is the initial Pu Content and $y_{M'}$ and $y_{M''}$ Are the Pu Contents in the Two Cubic Structures Observed for Each Sample after the Reducing Treatment, at Room Temperature, Estimated from Vegard's Law for Stoichiometric MOX (Except for MOX14, for Which the Origin of the Listed Values Is Given in the MO2+x Structure Section)[a]

name	y_{init} [mol %]	$y_{M'}$ [mol %]	Pu-rich [wt %]	$y_{M''}$ [mol %]	Pu-poor [wt %]	y_{calc} [mol %]	$y_{calc} - y_{init}$ [mol %]	$y_{M'} - y_{init}$ [mol %]
MOX14	14	70	10	8	90	8.6	5.4	6
MOX24	24	53	40	5	60	24.2	0.2	19
MOX35	35	53	60	5	40	33.8	1.2	30
MOX46	46	59	80	2	20	39.6	6.4	44
MOX54	54	57	85	1	15	48.6	5.4	53
MOX62	62	67	93	7	7	62.8	0.8	55

[a]The Pu-rich/poor weight percent is the weight fraction of the given cubic structure after reduction at room temperature from Rietveld refinement. y_{calc} is derived from the $y_{M'}/y_{M''}$ and Pu-rich/poor weight percent values. $y_{calc} - y_{init}$ is the difference between the calculated Pu content and the initial one. $y_{M'} - y_{init}$ is the difference between $y_{M'}$ and the initial Pu content.

changed to 60:40. The high Pu content of the Pu-rich phase, estimated at 53 mol % from Vegard's line, speaks in favor of the decrease in the O content below O/M = 2.00, causing the departure of the lattice parameter beyond the blue line. Considering the oxygen potential of the gas, the more the structure is rich in Pu, the lower its equilibrium O/M should be. Nevertheless, the sample returns to the stoichiometric composition upon cooling, which is dictated by the change in the equilibrium O/M, which at room temperature and under the considered atmosphere is exactly 2.00.

Assuming that both cubic structures were stoichiometric, their weight fractions 60 and 40 and their Pu contents 5 and 53 mol % estimated from Vegard's law correspond to the initial Pu content of 25 mol % at room temperature. This shows that the assumption of stoichiometry and estimations of both the weight percent and Pu content are precise.

MOX35. Evolution of the cubic lattice parameters and the weight percent of the orthorhombic phase are shown in Figure 7. In this case, reduction began at 673 K with the M_3O_8 structure reflections disappearing completely at 973 K. Similarly to what happened in the case of MOX24, the Pu-rich cubic phase was reduced slightly below the stoichiometric composition, but we assume that it became stoichiometric after cooling because of interaction with the gas. Also here, the assumption of stoichiometric structures at room temperature is correct because the weight fractions 40 and 60 and Pu contents 5 and 53 mol % correspond to an overall composition equal to the initial 35 mol % Pu.

MOX46. After oxidation in air, the sample was composed of 70 wt % cubic phase and 30 wt % orthorhombic phase. Reduction started at 673 K, and the orthorhombic structure reflections disappeared at 973 K. The Pu-rich cubic phase became stoichiometric at 1373 K, with the lattice parameter starting to overlap that of Martin's recommendation for 49 mol % Pu, which can be observed in Figure 8, where the lattice parameters of the two fluorite structures and M_3O_8 weight percent are plotted against the temperature. The Pu-poor cubic phase formed after reduction of M_3O_8 and followed Martin's recommendation for MOX with 1.5 mol % Pu at all times. After the thermal cycle, the sample consisted of 80 wt % Pu-rich and 20% Pu-poor cubic phases. The large difference between the initial and final ratios comes from the fact that the uncertainty of the weight percent value depends strongly on the amounts of the phases, as described at the beginning of this section. For cases where the ratio is close to 50:50, the error is much lower that, for example, here where the proportions are far from equal. We estimate the uncertainty in this case at 4 wt %. Also, the lattice parameter of the minority structure is more uncertain at 0.01 Å.

MOX54. After oxidation in air, the sample consisted of about 20 wt % orthorhombic and 80 wt % cubic phases. Evolution of the lattice parameter and the M_3O_8 weight percent during heat treatment are shown in Figure 9. The M_3O_8 reflections started to decrease in intensity at 773 K, and the structure was completely replaced by a cubic one at 973 K. At 1073 K, the Pu-rich structure lattice parameters started to overlap those of Martin's recommendation for MOX with 57 mol % Pu. The Pu-poor phase that formed from the M_3O_8 one had a lattice parameter that followed Martin's recommendation for MOX with 1 mol % Pu. The final ratio between the two phases was not equal to the initial one: the amount of the Pu-rich phase increased to 85 mol %.

MOX62. The material after oxidation consisted of 85 wt % cubic and 15 wt % orthorhombic phases. Evolution of the lattice parameter and the M_3O_8 weight percent during heat treatment are shown in Figure 10. Reduction started at 673 K, and the orthorhombic phase was gone by the time the sample reached 873 K.

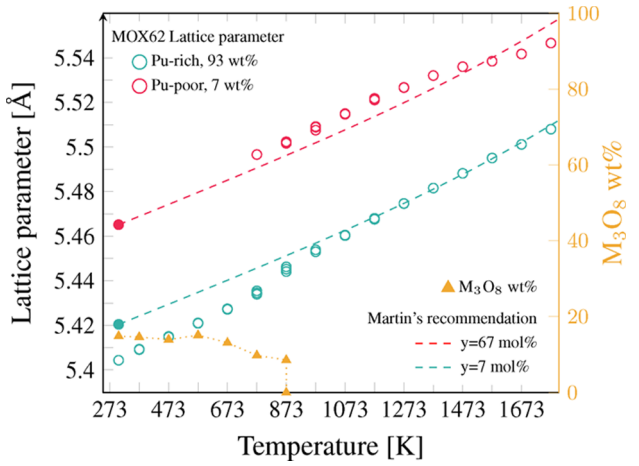

Figure 10. Lattice parameter and M_3O_8 weight percent plotted in temperature for MOX62. See the caption of Figure 6.

The Pu-rich cubic structure started to follow Martin's recommendation for MOX with 67 mol % Pu at 1173 K. The Pu-poor structure had a lattice parameter corresponding to pure UO_2 when it formed, and then it departed from Martin's recommendation for this composition and at room temperature the lattice parameter corresponded to 7 mol % Pu, based on a comparison with Vegard's law.

DOI: 10.1021/acs.inorgchem.5b01544
Inorg. Chem. 2015, 54, 9105−9114

DISCUSSION

Products of Oxidation. From the basic analysis of the obtained results presented in the previous section, we can propose an initial description of the oxidation products. In Table 2, we list the key parameters deduced from the results.

Oxidation of all samples resulted in two phase products, consisting of $M'O_{2+x}$ and $M_3''O_8$ structures. In principle, the ratio between the two depended only on the Pu content for samples with $y > 0.25$ because they were heated at the same temperature for the same period of time and in the same atmosphere. MOX14 was heated at a slightly lower temperature and for a shorter time; thus, a direct comparison with all of the other samples might result in incorrect conclusions. In Figures 11 and 12, the lattice parameter evolution of the cubic structures and the M_3O_8 weight percnt during the initial oxidation treatment were plotted as a function of time.

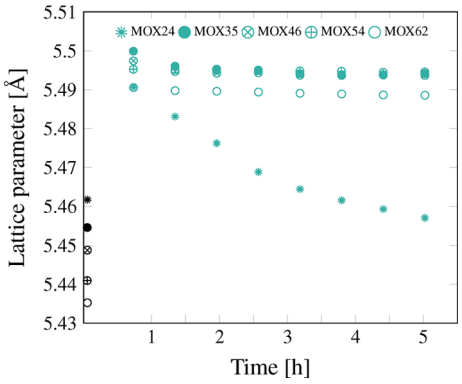

Figure 11. Cubic lattice parameter evolution in time during the oxidizing heat treatment for samples MOX24−MOX62. Points at $t = 0$ correspond to values at room temperature, measured before each treatment.

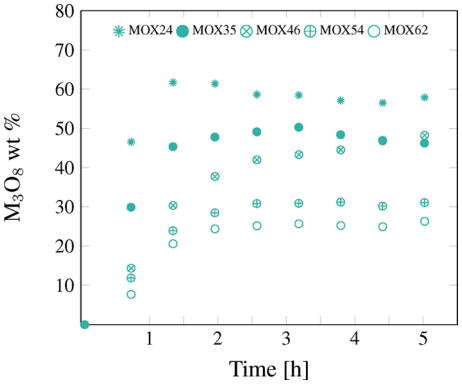

Figure 12. M_3O_8 weight percent in time during the oxidizing heat treatment for samples MOX24−MOX62.

One can notice differences between the M_3O_8 weight percent final value in Figure 12 and the ones given in Table 2. These were caused by the swelling of the sample during oxidation, which was discussed also in our previous study.[2] The values in the table are based on measurements taken after grinding of the oxidized powder, its redeposition on the heating strip, and calibration of the setup; thus, we treat them as the more accurate ones. Also, a strong departure from the general trend can be observed for MOX24 lattice parameter evolution. The diffraction patterns in this case were distorted because of the formation of large quantities of M_3O_8. After grinding and redeposition of the powder, the reflections became clearer, but the lattice parameter remained different from the others. In Figure 13, we plotted the weight percent of the M_3O_8 structure

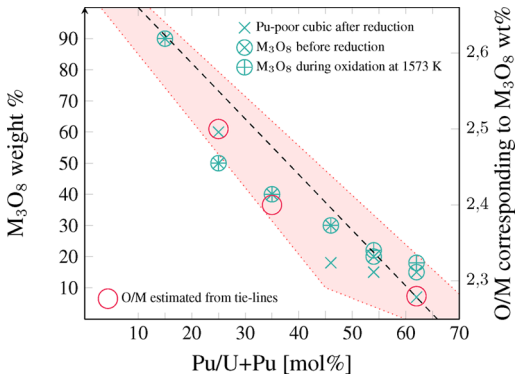

Figure 13. M_3O_8 weight percent and corresponding O/M plotted against the initial overall Pu content. The O/M value was estimated with the assumption that the cubic phase had an O/M of 2.25 and M_3O_8 2.66. The M_3O_8 during oxidation at 1573 K series was taken from ref 2. The dashed line joins the point corresponding to the estimated limit of plutonium miscibility in M_3O_8 at 1573 K with PuO_2. The red region is our estimate of the value that takes into account the experimental errors.

observed after oxidation against the Pu content of the sample (based on scans taken after grinding and redeposition). We also plotted the amount of M_3O_8 at 1573 K during oxidation from our previous study and the amount of the Pu-poor structure after reduction, estimated from the last recorded pattern at room temperature. The dashed line joins (O/M, y) points (2.66, 10) and (2.00, 100). The red circles correspond to the O/M values estimated from the position of the two samples MOX24 and MOX35 on one tie line (see the Tie Lines in the MO2+x−M3O8 Domain at 1573 K section).

With increasing initial Pu content, we observe a decrease in the M_3O_8 weight percent, which corresponds to a decrease in the amount of Pu-poor cubic phase observed after reduction. The same tendency was also noted in our previous study. Also, the results are quite similar if we compare M_3O_8 phase fractions after the oxidation treatment in this study and the ones observed at 1573 K during the slow oxidation described in ref 2. What is worth noting is the linear decrease in the O-rich phase fraction for samples with $y < 0.54$. If we fit the points with a linear trend and extrapolate it to 100 wt %, the corresponding Pu content will be 10 ± 5 mol %. To define the trend line, we took only the results from patterns taken after the reducing treatment for MOX24, MOX35, and MOX46 and, because we have observed the same value in the three presented data sets, the phase fractions for MOX14. The red area depicts the trend taking into account the uncertainties.

MO_{2+x} Structure. The assumption that the cubic phase in equilibrium with M_3O_8 is of the composition $MO_{2.25}$ is supported in the literature and our findings. It was confirmed in a previous study that the lattice parameter of the M_4O_9 phase does not change with global O/M for the studied Pu contents.[4] The results from our previous study[2] confirm this assumption, but no observation permitted us to associate the oxidized cubic structure with tetragonal M_4O_9. We observed an MO_{2+x} cubic structure, which was formed directly after the beginning of oxidation with a linear thermal expansion coefficient, slightly higher than that found for stoichiometric MOX. The fact that

DOI: 10.1021/acs.inorgchem.5b01544
Inorg. Chem. 2015, 54, 9105−9114

evolution of the lattice parameter of this structure was linear in temperature suggests that its O/M and Pu content did not change, although the global O/M was increasing through the continuous formation of M_3O_8. This description falls in line with what Markin and Street proposed as the behavior of the M_4O_9 phase, but also no superstructure peaks associated with this structure were observed. If we take its lattice parameter evolution determined in our previous study[2] in Table 3 and extrapolate it to room temperature, the values correspond to a theoretical Vegard plot joining U_4O_9 and PuO_2, which is shown in Figure 14.

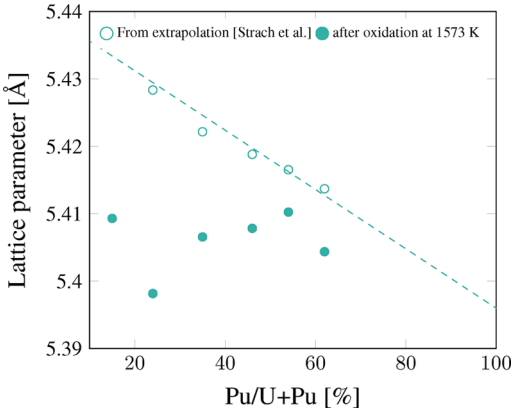

Figure 14. Empty circles correspond to lattice parameters at room temperature estimated by extrapolating the linear trends proposed for M_4O_9-like structures with different Pu contents in ref 2 in Table Table 2. The colored circles are lattice parameters measured before the reducing thermal treatment, i.e., after oxidation in air and redeposition of the resulting powders. The dashed line joins the lattice parameters of U_4O_9 and PuO_2.[13]

Markin and Streets observed a similar behavior but did not draw any conclusions from it. We propose that the line defines a limit for the lattice parameter of a MO_{2+x} structure in the presence of M_3O_8, in the instance when no cation transport was observed. If cation transport took place, causing a strong departure of Pu/U + Pu of the two constituting phases from the initial value, the limit seems to be invalid. If we take the lattice parameters of the Pu-rich cubic structure measured before the reducing heat treatment (after oxidation at 1573 K series in Figure 14) and compare it to the line joining U_4O_9 and PuO_2, we can obtain the Pu content of this structure, assuming that it reached the limit of oxidation in air. However, if we take these values and put them together with the phase fractions to determine the Pu content in the Pu-poor phase, it gives a reasonable value only for MOX14 (Table 2).

Reduction. After reduction, only two cubic structures remained, and in most cases, both followed Martin's recommendation for stoichiometric MOX compounds. In each case, one appeared to be rich and one poor in Pu, with the latter forming after the disappearance of the M_3O_8 reflections. This is clear evidence that the conditions of oxidation permitted cation migration. As mentioned at the beginning of the Results section, we estimated the Pu content of the two cubic phases based on a comparison with Vegard's law. This can only be done with the assumption that they were both stoichiometric, with O/M = 2.00, after the reduction took place.

The value of the oxygen partial pressure measured by our oxygen probe operating at 923 K was always between 10^{-24} and 10^{-27} atm. This low oxygen partial pressure is surely a result of the equilibrium reaction $H_2 + O_2 \rightarrow H_2O$, which was possible due to small impurities in the gas and a decrease in the p_{O_2} with our oxygen pump. Thus, to obtain the oxygen chemical potential value in the sample chamber, we first calculate the p_{H_2}/p_{H_2O} ratio from the measured p_{O_2}, and assuming that it stays constant in temperature, we calculate the value of the potential at the sample temperature using eq 3 given in ref 14.

$$\Delta\bar{G}_{f,H_2O}{}^{\circ} = -57250 + 4.48T \log T - 2.21T \quad [\text{in cal/mol of } H_2O] \tag{3}$$

We can compare these values with evolution of the oxygen potential of the different MOX compositions observed in this study at the highest temperature used, 1773 K. It has to be noted that we need to consider the Pu contents of the Pu-rich and -poor cubic structures, resulting from cation migration during oxidation, i.e., M′ and M″ in Table 2, rather than the initial Pu contents. It appears that at 1773 K the oxygen potential of the most reducing registered gas corresponded to a slight departure from O/M = 2.00, i.e., 1.95 for MOX with y = 0.7, which is shown in Figure 15.

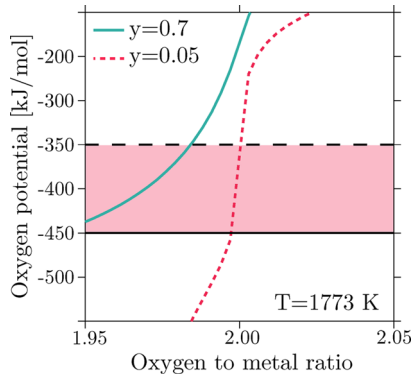

Figure 15. Plot of the oxygen potential of two different MOX compounds. The blue solid curve was calculated for MOX with y = 0.7 and the red dashed line for MOX with y = 0.05. The two horizontal lines mark the range of possible oxygen potentials in the sample chamber during the last plateau of the reducing treatment at 1773 K. The curves are based on Calphad predictions, using the TAFID thermodynamic database.

Using an equation given by Duriez[15]

$$a\ (\text{pm}) = 547.0 - 7.4y + 32x \tag{4}$$

to calculate the lattice parameter from the Pu content and departure from stoichiometry $(U_{1-y}Pu_y)O_{2-x}$ for O/M = 1.95 and y = 0.7, we obtain a difference in the lattice parameter between the stoichiometric and slightly reduced sample Δ = 0.016 Å. The same calculation for y = 0.05 and O/M = 1.998 gives Δ = 0.001 Å. At such low values we cannot neglect the fact that the oxygen partial pressure was not measured in the vicinity of the sample, but in an oxygen probe outside of the glovebox. Thus, the uncertainty of this measurement is quite high and that is the reason behind the wide range of oxygen potentials that we consider.

Nevertheless, in most of the cases, we observe that the samples do follow Martin's recommendations for stoichiometric MOX, which indicates that little or no reduction occurred. We observe slight departures for MOX24 at T > 1473

DOI: 10.1021/acs.inorgchem.5b01544
Inorg. Chem. 2015, 54, 9105−9114

K. The lattice parameters of the Pu-rich structure cross Martin's recommendation determined for the lattice parameter at room temperature recorded after reduction and increase slightly beyond it, which can be seen in Figure 6. The Pu-poor structure lattice parameters follow the recommendation for stoichiometric MOX with $y = 0.05$ throughout the heat treatment. Also, the initial Pu content corresponds well with the one calculated using the phase fractions and Pu contents of the two observed cubic structures, as mentioned before in the Results section. Thus, in this case, the Pu-rich structure was slightly reduced at high temperatures but returned to stoichiometry upon cooling. The same is true for MOX35, with a much slighter departure at elevated temperatures.

For MOX46, we note a slight decrease in the lattice parameter of the Pu-poor structure, in relation to Martin's recommendation. A decrease would normally correspond to an increase of O/M. In this case though, we should not observe any oxidation, even for pure UO_2, given the used gas mixture. Aside from changes in the composition, we can also anticipate the influence of high temperature on the correctness of calibration, which might result in slight changes of the positions of the peaks. The same behavior was observed for MOX54 and MOX62, with a quite profound departure in the case of the latter. Also, for MOX62 the lattice parameters of the Pu-poor structure just after its formation at 773 K fall on the line that corresponds to Martin's recommendation for pure UO_2. At a high temperature, we observe the mentioned departure downward from this line, and at room temperature after cooling, the lattice parameter can be assigned to a composition with $y = 0.07$ and O/M = 2.00. This might have been caused by cation migration, which resulted in an increase of the Pu content in the Pu-poor structure. Simultaneously, we should observe a decrease in Pu in the Pu-rich structure, but because the phase proportions are 7:93, such a slight change cannot be detected.

For MOX14, the two sets of low angle peaks—one corresponding to the fluorite MO_{2+x} phase and the other to the orthorhombic M_3O_8 phase—transform into one set corresponding to one fluorite structure. What has most likely happened is that the two phases did not, as it appears, form a solid solution once again, which is highly unlikely at the considered temperature (disappearance of the M_3O_8 peaks was observed at 1073 K), but rather the Pu-rich structure produced reflections too weak to emerge from underneath the high-intensity peaks of the Pu-poor structure, which formed from M_3O_8. It can be seen in Figure 16, where the patterns taken before and after the reducing heat treatment are shown at room temperature. Moreover, as the minority cubic phase was reduced, the position of the peak surely shifted toward lower angles, making it effectively impossible to distinguish the reflections coming from the minority and majority structures. This makes the determination of the miscibility of Pu in the M_3O_8 phase complicated in this case, and we can only state that it is surely below 14 mol % because the product of oxidation consisted of two phases. From a comparison of the theoretical Vegard's line joining U_4O_9 and PuO_2, we can estimate the Pu content of the Pu-rich structure at 70 mol % and the Pu-poor one at 8 mol %.

Tie Lines in the MO_{2+x}–M_3O_8 Domain at 1573 K. From the above results and discussion, we can deduce the approximate shape of the tie lines in the biphasic MO_{2+x}–M_3O_{8-z} domain of the U–Pu–O phase diagram at 1573 K.

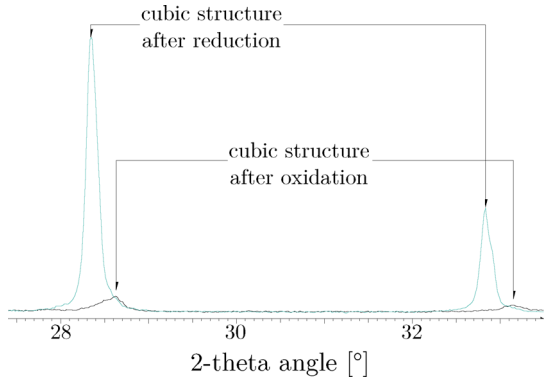

Figure 16. Fragments of two diffraction patterns taken at room temperature before and after the reducing heat treatment for MOX14. The angular range was chosen so that the (111) and (002) reflections of the cubic structure were visible. Assuming that the phase fractions did not change during the heat treatment, we can conclude that in the end two structures might have been present, with one set of reflections under the other. The y axis is the relative intensity.

The reduction of MOX24 and MOX35 resulted in the formation of two almost identical cubic structures, with different weight proportions. Thus, we can position the two samples on the same tie line at 1573 K, which was shown in Figure 17.

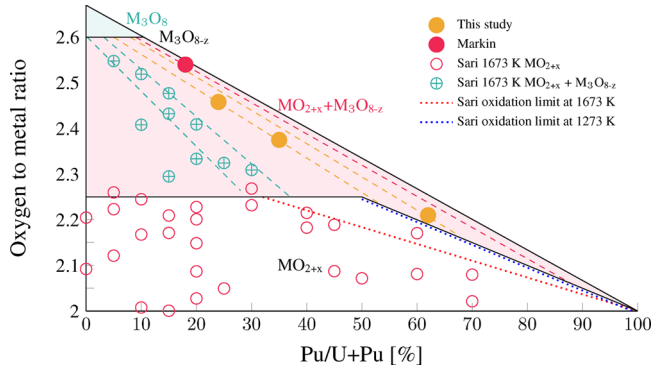

Figure 17. Fragment of the U–Pu–O phase diagram, with the biphasic MO_{2+x}–M_3O_{8-z} domains. Two tie lines at 1573 K, determined in this study, were marked according to the M′ and M″ values estimated for MOX24, MOX35, and MOX62. We assume the miscibility of Pu in M_3O_8 at 8 ± 2 mol % (Pu/U + Pu). Also shown are data points and tie lines reported by Benedict and Sari[7] and Markin and Street.[4] Marked in the dotted line are the limits of oxidation in air determined by Benedict and Sari[7] at two temperatures: 1273 and 1673 K.

The lower O/M limit for M_3O_{8-z} was taken after Benedict and Sari,[7] who found a single orthorhombic structure at almost the same O/M = 2.6 for uranium oxide and MOX with 5% Pu/U + Pu.

What can be deduced from this figure is that the slopes of the tie lines in this region (close to the line joining U_3O_8 and PuO_2) are quite similar and the anticipated slight differences would be hard to determine considering the uncertainties in our approach. One would expect that in the U-rich side of the phase diagram tie lines would be almost vertical, considering a certain miscibility of Pu in M_3O_8. For compounds with a Pu content only slightly higher than this limit, oxidation would

DOI: 10.1021/acs.inorgchem.5b01544
Inorg. Chem. 2015, 54, 9105–9114

then result in two phases with strong cation disproportions, which was observed in our study, supposedly also for MOX14.

The other samples could be placed on tie lines close to the one determined above, judging from the phase fractions and Pu contents, but the uncertainties are too high and the values do not correspond that well, as in the case of MOX24 and MOX35. We propose another tie line based on the results of MOX62.

These tie lines, extending to high Pu contents, are in accordance with the findings of Markin and Street[4] and Brett and Fox.[6] Sari et al.,[5] on the other hand, did not report such tie lines and questioned their existence based on their results. These authors also proposed a limit for the highest O/M achievable by oxidation in air for MOX with high Pu contents (shown in Figure 17 for 1273 and 1673 K obtained by quenching samples after prolonged heat treatment in air), which supposedly decreases at higher temperatures. The proof of its existence is supposed to be the fact that, after oxidation in air at a given temperature and quenching, the authors found a single cubic structure. We clearly obtained a biphasic product after oxidation in air of MOX54 and MOX62, which contradicts this theory. This difference might be an effect of the physical form of the samples in our study and that of Sari et al.[5] The authors used sintered pellets, while we perform the in situ diffraction on powders, which should enhance oxidation. Also the temperatures used were different. Markin and Street[4] propose the phase boundary for $y > 50\%$ to be slightly above the line joining U_2O_5 and PuO_2. If this is true, even for samples with a Pu content higher that 50% Pu/U + Pu, we should observe M_3O_8 upon oxidation, which we did. Thus, we propose the boundaries of the biphasic M_3O_{8-z}−MO_{2+x}/M_4O_9 domain, as shown in Figure 17.

Also in Figure 17, we show tie lines established by Sari for the U-rich region of the biphasic domain at 1673 K. These are much less tilted compared to the ones determined in this study, and also the Pu content in the M_3O_{8-z} structure was estimated to be lower.

We thus conclude that the Pu content in the two phases resulting from oxidation might depend strongly on the overall O/M of the sample. The point at which a given tie line meets the M_3O_8 single-phase domain might shift with only a slight change in the overall O/M of the compounds. With the degree of oxidation strongly dependent on the conditions during the heat treatment and the sample's composition, we can anticipate slight differences in the temperature or the oxygen partial pressure in the gas to cause strong changes in the M′ and M″ values of the resulting product. In other words, the reason why all of the studied samples did not form two structures with identical (independent of initial Pu content) values of M′ and M″, falling on the same tie line, was the fact that the border of the discussed biphasic domain (line joining U_3O_8 and PuO_2 with O/M = 2.00) has not been reached in all cases. The reasons might be oxidation kinetics or too low oxygen potential of the gas used.

Pu Miscibility in M_3O_8 at 1573 K. We can define the limit of solubility of Pu in M_3O_8 as the highest amount of this actinide that can be incorporated into the M_3O_8 structure at a certain temperature.

The maximum solubility of Pu in M_3O_8 can then be defined as the highest solubility of Pu in M_3O_8 under any conditions (T, p_{O_2}, etc.) or, in other words, the highest of all possible limits of solubility.

It is quite hard to discuss this value without any direct O/M measurements, but we can try to draw some conclusion from the available results, nevertheless.

Judging from Figure 13, oxidation in air at 1573 and 1373 K for MOX14 resulted in compounds with compositions close to the line joining M_3O_8 (with 10 mol % Pu/U + Pu, O/M = 2.66) and PuO_2 (O/M = 2.00). This line is the limit of oxidation of solid MOX compounds, beyond which oxidation continues with the formation of gaseous species. The fact that our MOX14 sample was supposedly close to this limit is of importance to this discussion because we found a biphasic product with different Pu contents in the two constituting structures in this case. If the limit of solubility of Pu in M_3O_8 was higher than 15 mol % at this temperature, we should obtain a single-phase product. From this observation, we can conclude that the limit of solubility is lower than 15 mol % Pu/U + Pu at 1373 and up to 1773 K, because during the oxidation described in ref 2, we observed two phases even at this higher temperature. Moreover, from the trend shown in Figure 13, we can estimate this limit as 8 ± 2 mol % at 1573 K.

A discussion of the maximum solubility of Pu in M_3O_8 would require a dedicated study at different temperatures of $1173 < T < 1473$ K on several samples with Pu contents of $1\% < y < 15\%$.

Phase Diagram at Room Temperature. Although the appearance of the hyperstoichiometric domain of the discussed ternary at room temperature has been proposed by Benedict and Sari,[7] the results might not be accurate because of the inhibited cation and anion diffusion at low temperatures. The authors mention that the room temperature representation was built based on the results from experiments in which samples were oxidized at a high temperature and subsequently slowly cooled to room temperature. The problem with this approach in the case of MOX is that during even slow cooling the anion and cation diffusion coefficients will decrease, finally preventing almost completely the transport of species at a certain T for a given cooling rate. This will result in a product equivalent to that obtained by quenching from said T. It is hard to judge the correctness of the results presented by Benedict and Sari[7] because the authors do not determine the cooling rate, only the duration of the isothermal plateau. We envisage a coupled thermogravimetric analysis/X-ray diffraction study to determine the temperature at which cation and anion transport stops.

■ CONCLUSIONS

On the basis of a thorough analysis of the lattice parameter evolution for the six studied compositions, we proposed a description of the oxidation behavior of MOX materials at 1573 K. For all of the six compositions studied with Pu contents between 14 and 62% Pu/U + Pu, the products of oxidation in air were two structures: cubic MO_{2+x} and orthorhombic M_3O_{8-z}. The samples were subsequently reduced in a controlled atmosphere to an O/M ratio of around 2.00 ± 0.05. This resulted in two stoichiometric cubic structures with different Pu contents. On the basis of a comparison with Vegard's law for stoichiometric MOX and the phase fraction from Rietveld refinement, we propose a description of the biphasic MO_{2+x}−M_3O_{8-z} region of the U−Pu−O phase diagram at 1573 K. We determined the positions of two tie line and coupled our results with literature data to give a better description of the tie lines' behavior in this domain. By using this modified approach, we were able to determine more precisely the limit of Pu miscibility in the orthorhombic structure at 8 ± 2 mol % Pu/U + Pu. We conclude that the

DOI: 10.1021/acs.inorgchem.5b01544
Inorg. Chem. 2015, 54, 9105−9114

swelling of samples due to M_3O_{8-z} formation strongly affects the diffraction patterns. The approach used in this study was successful in minimizing this impact and produced more accurate results compared to our previous study.[2]

AUTHOR INFORMATION

Corresponding Authors

*E-mail: strach@outlook.com.

*E-mail: renaud.belin@cea.fr.

Notes

The authors declare no competing financial interest.

REFERENCES

(1) Olander, D. *J. Nucl. Mater.* **2009**, *389*, 1−22.

(2) Strach, M.; Belin, R. C.; Richaud, J.-C.; Rogez, J. *Inorg. Chem.* **2014**, *53*, 12757−12766.

(3) Vauchy, R.; Robisson, A-Ch.; Martin, P. M.; Belin, R. C.; Aufore, L.; Scheinost, A. C.; Hodaj, F. *J. Nucl. Mater.* **2015**, *456*, 115−119.

(4) Markin, T.; Street, R. *J. Inorg. Nucl. Chem.* **1967**, *29*, 2265−2280.

(5) Sari, C.; Benedict, U.; Blank, H. *J. Nucl. Mater.* **1970**, *35*, 267−277.

(6) Brett, N.; Fox, A. *J. Inorg. Nucl. Chem.* **1966**, *28*, 1191−1203.

(7) Benedict, U.; Sari, C. European Atomic Energy Community (Euratom). *International Organisation and Integration*; Springer: Boston, MA, 1970.

(8) Dean, G. *Proc. Int. Conf. Plutonium, 3rd* **1965**, 806−827.

(9) Truphémus, T.; Belin, R. C.; Richaud, J.-C.; Reynaud, M.; Martinez, M.-A.; Félines, I.; Arredondo, A.; Miard, A.; Dubois, T.; Adenot, F.; Rogez, J. *J. Nucl. Mater.* **2013**, *432*, 378−387.

(10) *TOPAS V4: General profile and structure analysis software for powder diffraction data. User's manual*; Bruker AXS: Madison, WI, 2005.

(11) Martin, D. G. *J. Nucl. Mater.* **1988**, *152*, 94−101.

(12) Rietveld, H. M. *J. Appl. Crystallogr.* **1969**, *2*, 65−71.

(13) Sari, C.; Benedict, U.; Blank, H. *Proc. Symp. Thermodyn. Nucl. Mater. Emphasis Solution Syst.* **1967**, 587−611.

(14) Richardson, F. D.; Jeffes, J. H. E. *J. Iron Steel I.* **1948**, *160*, 261.

(15) Duriez, C.; Alessandri, J.-P.; Gervais, T.; Philipponneau, Y. *J. Nucl. Mater.* **2000**, *277*, 143−158.

DOI: 10.1021/acs.inorgchem.5b01544
Inorg. Chem. 2015, 54, 9105−9114